Catal Lett (2008) 121:165–171
DOI 10.1007/s10562-007-9316-1

Preparation, Characterization and Photocatalytic Activities of F-doped TiO_2Nanotubes

Ying Yu · Hai-Hong Wu · Bao-Lin Zhu · Shu-Rong Wang · Wei-Ping Huang · Shi-Hua Wu · Shou-Min Zhang

Received: 6 September 2007 / Accepted: 12 October 2007 / Published online: 30 October 2007

Abstract F-doped TiO_2 nanotubes were prepared by impregnation method. The prepared catalysts were characterized by XRD, TEM, and XPS. The photocatalytic activity of F-doped TiO_2 nanotubes was evaluated through the photodegradation of aqueous methyl orange. The experiments demonstrated that the F-doped TiO_2 nanotubes calcined at 300 °C possessed the best photocatalytic activity. Compared with pure TiO_2 nanotubes, the doping with F^- significantly enhanced the photocatalytic efficiency. The high photocatalytic activity was ascribed to several beneficial effects produced by F-doping: creation of oxygen vacancies, presence of Ti^{3+}, and so on.

Keywords F-doped TiO_2 · Nanotubes · Photocatalytic activity

1 Introduction

Titanium dioxide is an efficient photocatalyst in view of its strong oxidation activity. However, its photocatalytic oxidation rates for many target pollutants have been too slow to be of practical interest [1–3]. As such, considerable efforts have been made to improve the photocatalytic activity by doping ions into TiO_2 [4, 5]. Compared with metal cation dopants, nonmetal dopants may be more appropriate for the enhancement of photocatalytic activity of TiO_2 because their impurity states are near the valence band edge, they do not act as charge carriers, and their role as recombination centers might be minimized [6]. To date, some nonmetal such as nitrogen [7], carbon [8, 9], sulfur [10], phosphorus [11], and halogen atoms [12] etc. have been investigated.

Among them, fluorine-doped TiO_2 has been intensively researched. Hattori et al. prepared F-doped TiO_2 films [13–15]. The photoreactivity of TiO_2 films is enhanced significantly with F-doping, which is attributed to the increase in the rate at which the photogenerated charge carriers reach the surface in the photostationary state. Minero et al. [16, 17] studied photocatalytic transformation of organic compounds on a titanium dioxide-fluorine system. They confirmed that fluorine enhances the photocatalytic activity of TiO_2 powders for the photodecomposition of phenol in aqueous solution. Ayllón prepared anatase powders from fluorine-complexed titanium (IV) aqueous solution using microwave irradiation [18]. Yamaki et al. [19, 20] demonstrated the effects of F implantation in TiO_2 rutile single crystals followed by thermal annealing. Yu et al. [21, 22] synthesized mesoporous F-doped TiO_2 powders by hydrolysis of titanium tetraisopropoxide in a mixed NH_4F-H_2O solution. They reported that the crystallization of anatase is obviously enhanced due to F-doping. The photocatalytic activity of F-doped TiO_2 powders prepared by this method exceeds that of Degussa P25. Park and Choi [23] confirmed that the remote photocatalytic degradation of stearic acids is markedly faster with the surface-fluorinated TiO_2 film than with the pure TiO_2 film. Park and Choi [24] reported that F-doped TiO_2 is more effective than pure TiO_2 for the photocatalytic oxidation of Acid Orange 7 and phenol, but less effective for the degradation of dichloroacetate. Li et al. [25, 26] prepared F-doped TiO_2 powders by spray pyrolysis from an aqueous solution of H_2TiF_6. These F-doped TiO_2 powders exhibit very high visible-light

Y. Yu · H.-H. Wu · B.-L. Zhu · S.-R. Wang · W.-P. Huang · S.-H. Wu · S.-M. Zhang (✉)
Department of Chemistry, NanKai University, Tianjin 300071, China
e-mail: zhangsm@nankai.edu.cn

photocatalytic activity for decomposition of acetaldehyde and trichloroethylene. Ho et al. [27] also reported that hierarchical porous F-doped TiO_2 spheres were fabricated. The photocatalysts show high visible light photocatalytic activity on the degradation of 4-chlorophenol. Murakami et al. [28] synthesized highly active TiO_2 photocatalyst samples (containing Ti^{3+} species) by hydrothermal crystallization in organic media and post-calcination. Mori et al. [29] also synthesized TiO_2 photocatalysts by hydrothermal method from tetraisopropyl orthotitanate in the presence of NH_4F. The TiO_2 samples with high F^- ion contents exhibit high absorption in the UV-visible range with a shift to the longer wavelength in the band gap transition, and exhibit high photocatalytic activity for the degradation of *i*-BuOH. From these researches, it can be inferred that the introduction of fluorine really enhances the photocatalytic activity of TiO_2.

Recently, extensive researches have been conducted on the synthesis and characterization of TiO_2 nanotubes because of their novel properties such as unique shape, size confinement in radial-direction and large specific surface area [30–32]. Ion-doped TiO_2 nanotubes have been studied by some groups [33, 34]. However, to our knowledge, photocatalysis upon F-doped TiO_2 nanotubes has not been reported. In this paper, F-doped TiO_2 nanotubes were prepared by impregnation method, and characterized by the methods of XRD, TEM, and XPS. The photocatalytic activity of the F-doped TiO_2 nanotube catalysts was evaluated through the photodegradation of the methyl orange.

2 Experimental

2.1 Preparation of F-doped TiO_2 Nanotubes

TiO_2 nanoparticles were prepared by mixing a solution of tetrabutyl titanate (Analytical reagent) in ethanol with a solution of ethanol in water (water vs. EtOH ratio is 1:15). The mixture was kept under constant stirring at room temperature until complete hydrolysis. The gel was obtained by aging for 12 h at room temperature. The resulting gel was dried at 80 °C for 12 h. After the dried material was calcined in air at 500 °C for 3 h, TiO_2 nanoparticles were obtained.

TiO_2 nanotubes were synthesized via a hydrothermal chemical process as reported by Kasuga [30]. Typically, 1.2 g TiO_2 nanoparticles were mixed with 58 mL 10 mol L^{-1} NaOH aqueous solution in a Teflon vessel at 150 °C for 10 h. After the hydrothermal reaction, a white precipitate was centrifuged and washed with 0.1 mol L^{-1} HNO_3 to neutralize it, and then the precipitate was washed with distilled water. White TiO_2 nanotubes were obtained after drying at 80 °C in air.

F-doped TiO_2 nanotubes were synthesized from TiO_2 nanotubes by impregnation method. TiO_2 nanotubes were immersed into an aqueous NH_4F solution for 24 h to dope with fluorine. The obtained powders were centrifuged, then dried in air at 80 °C for 1 h, and calcined at different temperature for 2 h.

2.2 Characterization of F-doped TiO_2 Nanotubes

X-ray powder diffraction (XRD) analysis was performed using a Rigaku D/MAX-2500 X-ray diffractometer (CuKα $\lambda = 0.154$ nm). The working voltage and current of the X-ray tube were 40 kV and 100 mA. TEM images were obtained with a Philips T20ST transmission electron microscopy working at 200 kV. X-ray photoelectron spectra (XPS) were recorded on a PHI-1600 spectrometer (USA) equipped with a Mg Ka radiation for exciting photoelectrons. X-ray source was operated at 15 kV and 250 W. The pressure was 8×10^{-10} Torr (1 Torr = 133.33 Pa) during data acquisition. All binding energies (BE) were referenced to the adventitious C 1s line at 284.6 eV (1 eV = 1.602×10^{-19} J). Argon-ion etching of the catalyst was carried out for 20 min at 2 kV.

2.3 Photocatalytic Activity Measurement

The photocatalytic activity of the prepared catalysts was evaluated by the degradation rates of methyl orange (20 mg/L) in an aqueous solution (100 mL) containing 50 mg of sample. The reaction mixture was ultrasonically dispersed for 30 min, and then irradiated by using a 300 W High-Pressure Mercury Lamp under stirring. After every given irradiation time, a sample of 5 mL suspension was withdrawn, centrifugated and filtered. The obtained solution was then measured for checking the residual concentration of methyl orange with a UV-vis spectrophotometer (TU-1901) at 463.8 nm, which is the maximum absorption of methyl orange. The results are corrected for the decomposition of the dye in the absence of catalysts and for absorption of dye on the catalyst.

3 Results and Discussion

3.1 Crystal Structure

Figure 1 shows the XRD pattern of the F-doped and pure TiO_2 nanotubes calcined at 300 °C for 2 h. The diffractograms revealed that the pure TiO_2 nanotubes possessed the anatase phase (JCPDS 21-1272). XRD patterns of F-doped

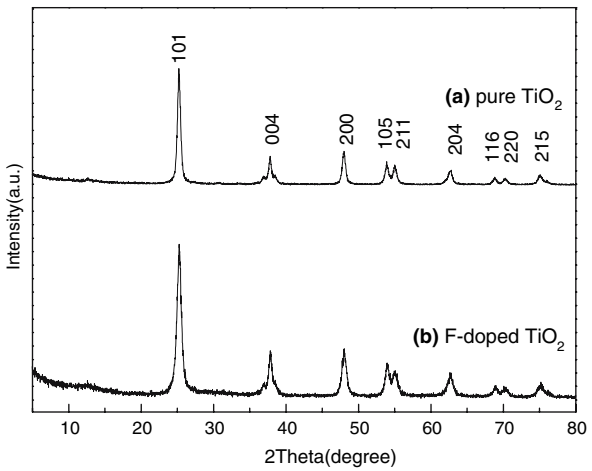

Fig. 1 XRD pattern of (**a**) pure TiO_2 nanotubes; (**b**) F-doped TiO_2 nanotubes

TiO_2 nanotubes only show all the main characteristic peaks of TiO_2, and no characteristic reflections for F or F containing phases were observed, indicating that fluorine was highly dispersed on TiO_2, or XRD was not sensitive enough to detect such minor changes to TiO_2.

Figure 2 shows TEM images of the F-doped TiO_2 nanotubes. Nanotubular structures were clearly observed. The nanotubes were nearly uniform. They were hollow and open-ended, and their length was more than one hundred of nanometers, similar to the results reported by Kasuga [30]. The multilayer nanotube structure had an outer diameter of 8–10 nm and inner diameter of 5–7 nm (Fig. 2b). It seems that the nanotubes are formed through scrolling the TiO_2 layer sheet, which can be concluded from the different wall number on different side (marked with arrows in Fig. 2b). The wrapping mechanism of a single nanosheet has also been favored by a number of groups [32]. Figure 2c shows the TEM image of the F-doped TiO_2 nanotubes calcined at 300 °C for 2 h. It can be seen that most of the nanotubes kept their tubular texture after the calcination process. Higher calcination temperature caused obvious damage of the nanotubes. Figure 2d shows the TEM image of the F-doped TiO_2 nanotubes calcined at 400 °C for 2 h. It can be observed

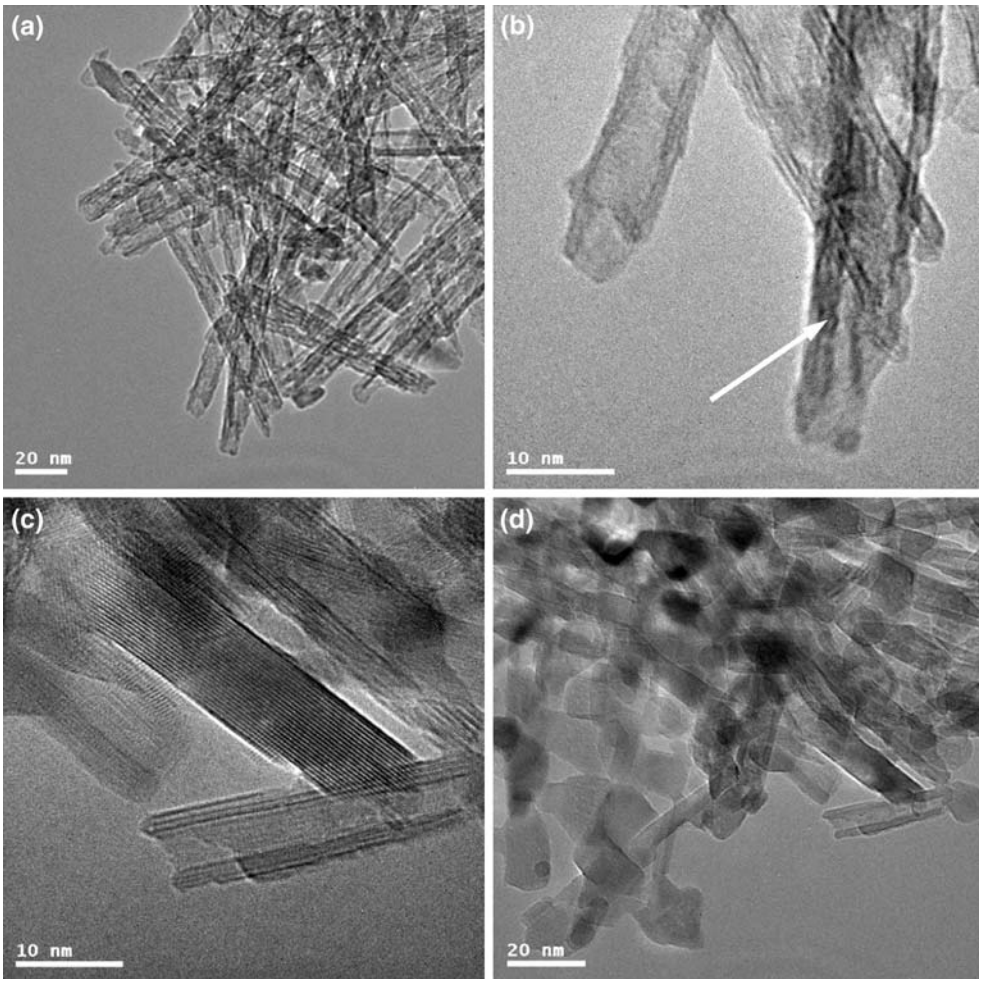

Fig. 2 TEM images of F-doped TiO_2 nanotubes without calcination (**a**, **b**), calcined at 300 °C for 2 h (**c**), and calcined at 400 °C for 2 h (**d**)

that most of the nanotubes are broken and aggregated. It seems that higher calcination temperature will induce the decrease of the catalytic activity.

3.2 XPS Studies

Figure 3a shows the XPS survey spectra before and after Ar^+ etching of F-doped TiO_2 nanotubes calcined at 300 °C for 2 h. There were Ti, O, F, and C on the surface of F-doped TiO_2. No noticeable signals assignable to N 1s binding energy could be observed, suggesting that N atoms originating from NH_4F were scarcely present. The C 1s peak is at 285.8 eV. The residual carbon resulted from the organic precursors used in the sol–gel method and was not completely removed during the heat treatment. The adventitious hydrocarbon from XPS itself may also cause the presence of C element. Compared with the sample before etching, the intensity of C 1s peak in the sample after etching was obviously weaker, indicating that the adventitious hydrocarbon from XPS itself was partly removed by Ar^+ etching.

The doping concentration of F analyzed by XPS was 4.11 wt.% before etching and was 2.88 wt.% after etching, which implied that F dopant had a much higher concentration at the exterior than that at the interior of TiO_2 nanotubes. The work mechanism of impregnation treatment may be the reason for the above result. In this process, F^- ions firstly adsorb mostly and strongly on the surface of TiO_2 nanotubes due to their very high surface area and strong electrostatic interaction, and then diffuse gradually into the lattices of TiO_2 nanotubes during the long impregnation time because F^- ionic radius is very small (133 pm). Therefore, the content of F^- decreases in the direction of the diffusion, from the exterior to the interior. It should be emphasized that the distribution of F^- ion here is different from that of heavy metal ions with impregnation method, in which case the heavy metal ions are limited at the surface of TiO_2 particles.

Figure 4 shows the high resolution XPS spectra of Ti 2p. The Ti $2p_{1/2}$ and Ti $2p_{3/2}$ spin-orbital splitting photoelectrons for both samples were located at binding energies of 464.2 and 458.7 eV respectively, which was in agreement with the reported literature values [35, 36], showing the presence of Ti^{4+}. However, the surface spectrum of the

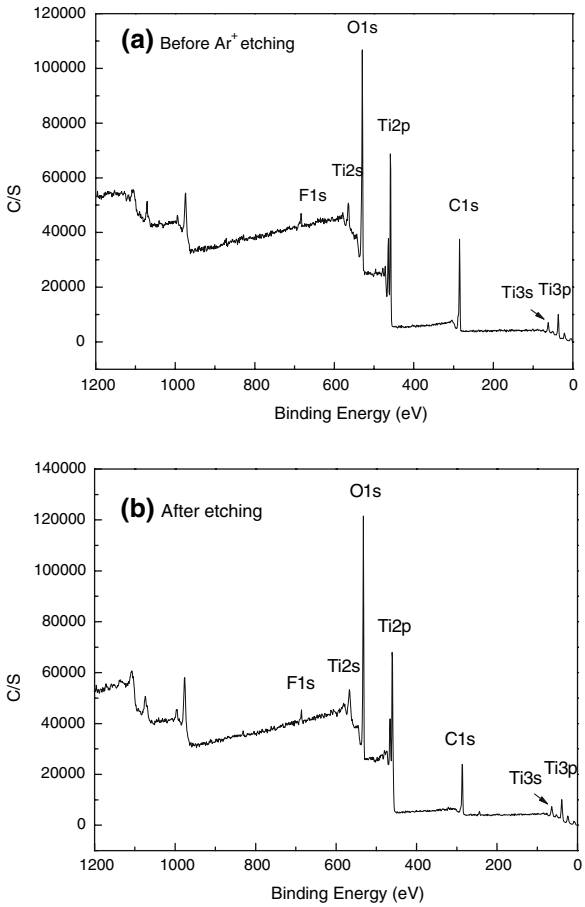

Fig. 3 XPS survey spectra of F-doped TiO_2 nanotubes before and after Ar^+ etching

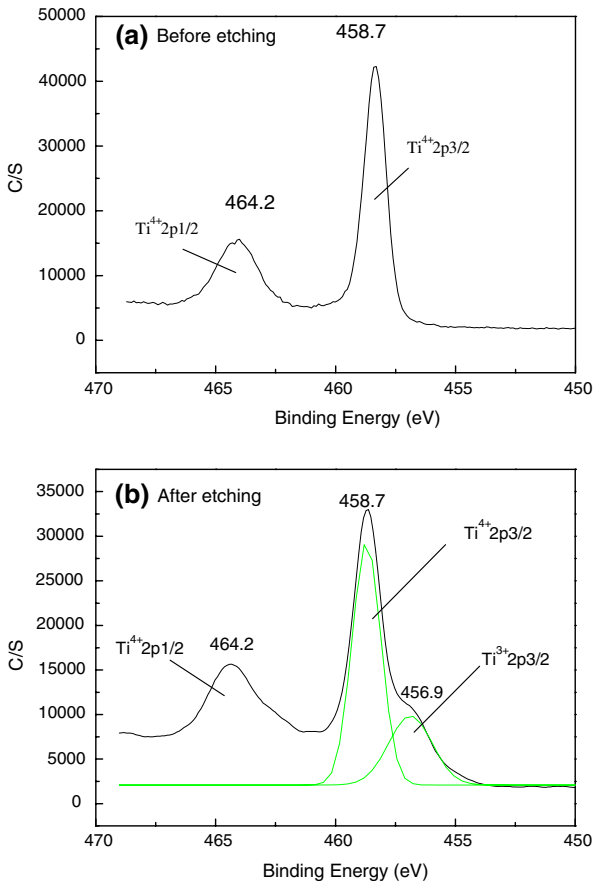

Fig. 4 High resolution XPS spectra of the Ti 2p region for the F-doped TiO_2 nanotubes before and after Ar^+ etching

etched sample revealed a shoulder region at 456.9 eV. An additional peak ascribed to Ti^{3+} 2p3/2 could be identified, suggesting the presence of Ti^{3+} species in the sample [35].

Ti^{3+} on the TiO_2 surface can be created by several methods such as UV radiation, annealing in vacuum, ion sputtering, plasma-treating and ion-doping [35, 37–39]. Yu et al. [21] reported that F^- doping in the lattice can convert some Ti^{4+} to Ti^{3+} originated from the charge compensation caused by the replacement of F^- ions with O^{2-} ions in the lattice. Jun et al. [40] reported that when TiO_2 samples are exposed to argon plasma, the energetic argon ions, electrons, neutrals and plasma radiation can take out adsorbed water from the surface and convert the Ti^{4+} state to Ti^{3+}. In this study, the most possible mechanism to account for the presence of Ti^{3+} might involve fluorine doping and/or Ar^+ etching.

The F 1s XPS spectrum of F-doped TiO_2 nanotubes before etching is similar to that after etching, as shown in Fig. 5. The F 1s region was composed of two contributions. One peak located at 684.7 eV was assigned to F^- ions physically absorbed on the surface of TiO_2; while that at 688.9 eV was ascribed to the F in solid solution $TiO_{2-x}F_x$, i.e. the substitute F^- ion that occupied oxygen sites in the TiO_2 crystal lattice [21, 41]. It is reasonable to assume that the small peak was resulted from Ti–F bonds, meaning that F^- ions were incorporated into TiO_2 lattice by the impregnation method.

Figure 6 shows the O 1s XPS spectra of F-doped TiO_2 nanotubes. For the sample before etching, the O 1s spectrum was asymmetric. Besides the main peak of O 1s located at about 530.0 eV corresponding to lattice oxygen of TiO_2 [O=], two shoulder peaks at higher binding energy could be identified. The peak at 531.4 eV should be attributed to the surface species, such as Ti–OH and Ti–O–O– [O=]. Generally, narrow scan O 1s XPS spectrum requires only two peaks (two oxidation states associated

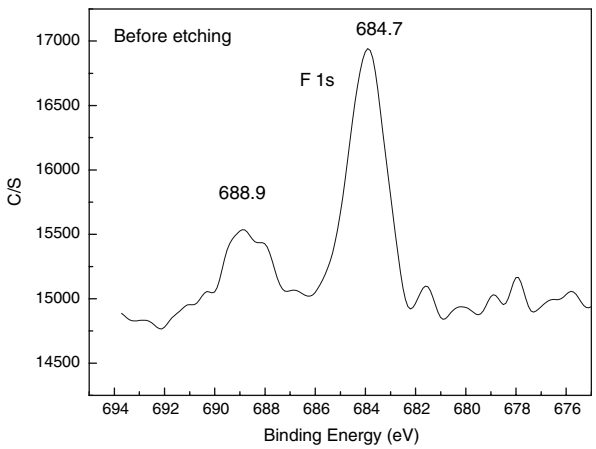

Fig. 5 High resolution XPS spectra of the F 1s region for the F-doped TiO_2 nanotubes before and after Ar^+ etching

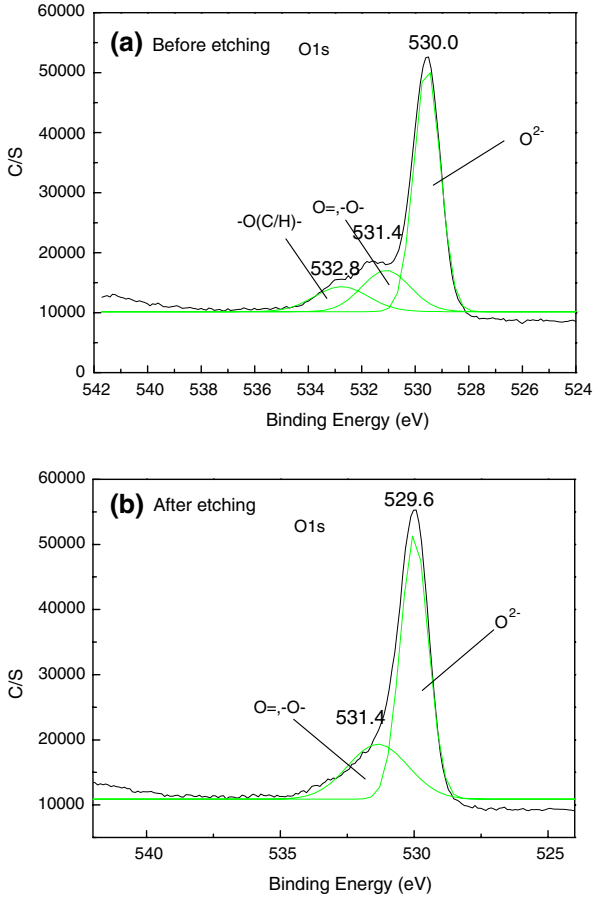

Fig. 6 High resolution XPS spectra of the O 1s region for the F-doped TiO_2 nanotubes before and after Ar^+ etching

with [O=] and [–O–]) to fit the curve [36, 40]. In this, the observed O 1s spectrum required one more peak at 532.8 eV to fit the extended bump at higher binding energy in the spectrum. Jun et al. [40] suggested that the peak at 532.8 eV possibly is attributed to [–O(H/C)–]. It can be due to water molecules remained at the TiO_2 surface, and/or carbon at the surface as an impurity. After Ar^+ etching treatment, the third peak [–O(H/C)–] in O 1s approximately disappeared, which indicated the removal of water and carbon from the TiO_2 surface. As shown in the survey XPS spectra, intensity of the peak corresponding to C 1s in the sample after etching was obviously weaker than that in the sample before etching.

3.3 Photocatalyic Activity

Calcination is an effective treatment method to enhance the photocatalytic activity of nanosized TiO_2 photocatalysts. Figure 7 shows the degradation rates of methyl orange for F-doped TiO_2 nanotubes calcined at different temperature for 2 h. It was evident that TiO_2 nanotubes calcined at

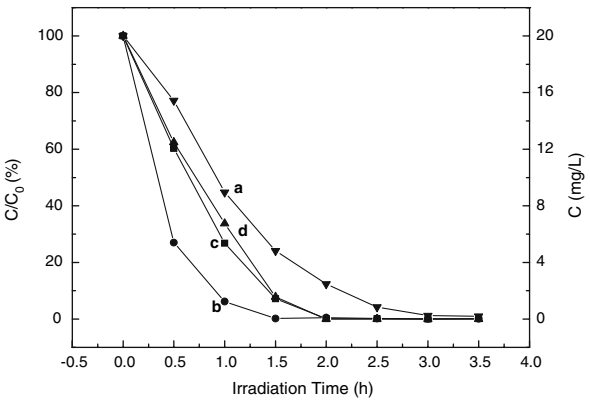

Fig. 7 The photodegradation of methyl orange for F-doped TiO_2 nanotubes calcined at different temperature for 2 h (**a**) 200 °C; (**b**) 300 °C; (**c**) 400 °C; (**d**) 500 °C

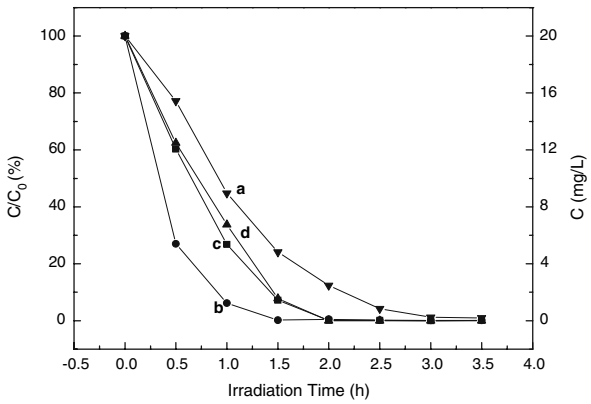

Fig. 8 Photocatalytic activity of (**a**) pure TiO_2 nanotubes; (**b**) F-doped TiO_2 nanotubes

200 °C (Fig. 7a) showed much lower photocatalytic activity than those calcined at 300 °C for degradation of methyl orange. Methyl orange was completely degraded after 2 h irradiation. Its low photoactivity may be attributed to the uncompleted complex decomposition on nanotubes' surface, which blocked the degradation reaction [34]. The F-doped TiO_2 nanotubes calcined at 300 °C possessed the best photocatalytic activity (Fig. 7b). Methyl orange was completely degraded within 1.5 h. This result is also in accordance with the result that is reported by Zhang et al. [42]. They reported that regarding the photo-degradation of propylene, TiO_2 nanotubes treated at 300 °C possess the best photocatalytic ability among the thermally treated TiO_2 nanotubes. F-doped TiO_2 nanotubes calcined at 400 °C exhibited a lower photoactivity than that calcined at 300 °C (Fig. 7c), which was similar to that calcined at 200 °C. The F-doped TiO_2 nanotubes calcined at 500 °C possessed the lowest photocatalytic activity (Fig. 7d). Methyl orange was completely degraded within 3 h. That is probably due to the agglomeration and sintering damage of nanotubes caused by calcination at high temperature [34]. With the increased calcinations temperature, the increased rutile content should be another reason for the weak performance.

Figure 8 shows the photocatalytic activity of pure and F-doped TiO_2 nanotubes calcined at 300 °C for 2 h. It is obvious that the doping of TiO_2 nanotubes with fluorine significantly enhanced the photocatalytic efficiency as compared with pure TiO_2 nanotubes. Methyl orange could be degraded completely within 1.5 h for F-doped TiO_2 nanotubes, while only 47.4% of methyl orange was degraded for pure TiO_2 nanotubes. Even if methyl orange was irradiated for 3.5 h, only 82.0% of methyl orange was degraded when pure TiO_2 nanotubes were used.

The doped-F atoms can promote the formation of oxygen vacancies. The role of oxygen vacancies is to directly provide the formation sites of active species for photocatalytic reaction. The formation of $O_2^{\bullet-}$ from chemisorbed oxygen or $OH^{\bullet}$ from adsorbed water requires the presence of surface oxygen vacancies. Minero et al. [16, 17] reported that the formation of $OH^{\bullet}$ is favored on fluorinated TiO_2. Thus, F-doping creates new active sites for $OH^{\bullet}$ formation.

The presence of Ti^{3+} can apparently enhance the photocatalytic activity. The oxygen molecule was adsorbed separately on the Ti^{3+} sites. As a matter of fact, the increased Ti^{3+} sites substantially resulted in increased oxygen adsorption, and then photooxidation [37]. In addition, the Ti^{3+} surface states may trap the photogenerated electrons and then transfer them to O_2 adsorbed on the surface of TiO_2. Therefore, the existence of a certain amount of Ti^{3+} surface states in TiO_2 results in the reduction of the electron and hole recombination rate, and enhanced photocatalytic activity [21, 37].

Consequently, the high photocatalytic activity of F-doped TiO_2 nanotubes is ascribed to several beneficial effects produced by F-doping: creation of oxygen vacancies, presence of Ti^{3+}, and so on.

4 Conclusions

F-doped TiO_2 nanotubes were prepared by impregnation method. The F-doped and pure TiO_2 nanotubes possessed the anatase phase. The nanotubes were hollow and open-ended, and their length was more than one hundred of nanometers. The doping concentration of F was 4.11 wt.% before Ar^+ etching and 2.88 wt.% after etching. There was a certain amount of Ti^{3+} species in the etched sample. The doped fluorine existed in two chemical forms, one was the F^- ions physically absorbed on the surface of TiO_2, and another was the substitute F^- ion that occupied oxygen sites in the TiO_2 crystal lattice.

The F-doped TiO_2 nanotubes calcined at 300 °C possessed the best photocatalytic activity. The doping with fluorine significantly enhanced the photocatalytic efficiency of TiO_2 nanotubes, which is ascribed to creation of oxygen vacancies, presence of Ti^{3+}, and so on.

References

1. Linsebigler AL, Lu GQ, Yates JT (1995) Chem Rev 95:735
2. Fujishima A, Rao TN, Tryk DA (2000) J Photochem Photobiol C 1:1
3. Diebold U (2003) Surf Sci Rep 48:53
4. Anpo M, Dohshi S, Kitano M, Hu Y, Takeuchi M, Matsuoka M (2005) Annu Rev Mater Res 35:1
5. Lindgren T, Mwabora JM, Avendano E, Jonsson J, Hoel A, Granqvist CG, Lindquist SE (2003) J Phys Chem B 107:5709
6. Wang H, Lewis JP (2006) J Phys: Condens Matter 18:421
7. Asahi R, Morikawa T, Ohwaki T, Aoki K, Taga Y (2001) Science 293:269
8. Sakthivel S, Kisch H (2003) Angew Chem Int Ed 42:4908
9. Choi Y, Umebayashi T, Yoshikawa M (2004) J Mater Sci 39:1837
10. Tian FH, Liu CB (2006) J Phys Chem B 110:17866
11. Yu HF (2007) J Phys Chem Solids 68:600
12. Hong XT, Wang ZP, Cai WM, Lu F, Zhang J, Yang YZ, Ma N, Liu YJ (2005) Chem Mater 17:1548
13. Hattori A, Yamamoto M, Tada H, Ito S (1998) Chem Lett 8:707
14. Hattori A, Shimoda K, Tada H, Ito S (1999) Langmuir 15:5422
15. Hattori A, Tada H (2001) J Sol–Gel Sci Technol 22:47
16. Minero C, Mariella G, Maurino V, Pelizzetti E (2000) Langmuir 16:2632
17. Minero C, Mariella G, Maurino V, Vione D, Pelizzetti E (2000) Langmuir 16:8964
18. Ayllón JA, Peiró AM, Saadoun L, Vigil E, Domènech X, Peral J (2000) J Mater Chem 10:1911
19. Yamaki T, Sumita T, Yamamoto S (2002) J Mater Sci Lett 21:33
20. Yamaki T, Umebayashi T, Sumita T, Yamamoto S, Maekawa M, Kawasuso A, Itoh H (2003) Nucl Instrum Meth Phys Res B 206:254
21. Yu JC, Yu JG, Ho W, Jiang ZT, Zhang LZ (2002) Chem Mater 14:3808
22. Yu JG, Yu JC, Cheng B, Hark SK, Iu K (2003) J Solid State Chem 174:372
23. Park JS, Choi W (2004) Langmuir 20:11523
24. Park H, Choi W (2004) J Phys Chem B 108:4086
25. Li D, Haneda H, Labhsetwar NK, Hishita S, Ohashi N (2005) Chem Phys Lett 401:579
26. Li D, Haneda H, Hishita S, Ohashi N, Labhsetwar NK (2005) J Fluorine Chem 126:69
27. Ho W, Yu JC, Lee S (2006) Chem Commun 10:1115
28. Murakami SY, Kominami H, Kera Y, keda S, Noguchi H, Uosaki K, Ohtani B (2007) Res Chem Intermed 33:285
29. Mori K, Maki K, Kawasaki S, Yuan S, Yamashita H, Chem Eng Sci in press
30. Kasuga T, Hiramatsu M, Hoson A, Sekino T, Niihara K (1998) Langmuir 14:3160
31. Macak JM, Tsuchiya H, Schmuki P (2005) Angew Chem Int Ed 44:2100
32. Yao BD, Chan YF, Zhang XY, Zhang WF, Yang ZY, Wang N (2003) Appl Phys Lett 82:281
33. Vitiello RP, Macak JM, Ghicov A, Tsuchiya H, Dick LFP, Schmuki P (2006) Electrochem Commun 8:544
34. Xu JC, Lu M, Guo XY, Li HL (2005) J Mol Catal A 226:123
35. Liu HM, Yang WS, Ma Y, Cao YA, Yao JN, Zhang J, Hu TD (2003) Langmuir 19:3001
36. Nagaveni K, Hegde MS, Ravishankar N, Subbanna GN, Madras G (2004) Langmuir 20:2900
37. Suriye K, Praserthdam P, Jongsomjit B (2007) Appl Surf Sci 253:3849
38. Hengerer R, Bolliger B, Erbudak M, Gratzel M (2000) Surf Sci 460:162
39. Guillemot F, Porte MC, Labrugere C, Baquey C (2002) J Colloid Interface Sci 255:75
40. Jun J, Shin JH, Dhayal M (2006) Appl Surf Sci 252:3871
41. Huang DG, Liao SJ, Liu JM, Dang Z, Petrik L (2006) J Photochem Photobiol A 184:282
42. Zhang M, Jin ZS, Zhang JW, Guo XY, Yang JJ, Li W, Wang XD, Zhang ZJ (2004) J Mol Catal A 217:203